Continuous phase transition and negative specific heat in finite nuclei

J. N. De,[1,2] S. K. Samaddar,[1] S. Shlomo,[2] and J. B. Natowitz[2]
[1]*Saha Institute of Nuclear Physics, 1/AF Bidhannagar, Kolkata 700064, India*
[2]*The Cyclotron Institute, Texas A&M University, College Station, Texas 77843, USA*
(Received 19 July 2004; revised manuscript received 14 October 2004; published 8 March 2006)

The liquid-gas phase transition in finite nuclei is studied in a heated liquid-drop model where the nuclear drop is assumed to be in thermodynamic equilibrium with its own evaporated nucleonic vapor, conserving the total baryon number and isospin of the system. It is found that in the liquid-vapor coexistence region the pressure is not a constant on an isotherm, indicating that the transition is continuous. At constant pressure, the caloric curve shows some anomalies; namely, the systems studied exhibit negative heat capacity in a small temperature domain. The dependence of this specific feature on the mass and isospin of the nucleus, Coulomb interaction, and the chosen pressure is studied. The effects of the presence of clusters in the vapor phase on specific heat have also been explored.

DOI: 10.1103/PhysRevC.73.034602 PACS number(s): 25.70.Pq, 24.10.Pa, 64.60.Ak

I. INTRODUCTION

The possible occurrence of a liquid-gas phase transition in atomic nuclei has aroused intense interest in recent times. For macroscopic extensive systems, phase transitions are well defined. For microscopic systems, nuclei for example, the presence of the surface and the long-range Coulomb interaction adds complexities in defining the liquid-gas-type phase transition normally reserved for extensive infinite systems. However, over the years, there has been a large buildup of theoretical data in different models, including statistical multifragmentation [1–3], percolation [4], lattice-gas [5,6], and microscopic finite-temperature Thomas-Fermi [7] models that are largely in consonance with the occurrence of a liquid-gas-type phase transition in finite nuclei. Experiments [8,9] on nucleus-nucleus collisions also give signatures like the critical-like behavior of the observed fragment partitions—the nearly flat caloric curve, leading to a peaked structure in the specific heat—that are compatible with the occurrence of such a transition in finite nuclei. A coherent characterization of its properties such as the phase diagram or the order of the phase transition has not, however, clearly emerged yet.

In a microcanonical statistical multifragmentation model, with canonical input for fragment formation probability, Bondorf *et al.* [1] noted some anomalous behavior in the caloric curve in the excitation energy range from 3 to 5 MeV/nucleon, where the slope of the curve is negative. In a microcanonical sampling of statistical multifragmentation, Gross [3] noted an anomalous behavior in the caloric curve leading to negative specific heat. Such a behavior was also seen in a microcanonical ensemble of a symmetric $A = 36$ nuclear system prepared with antisymmetrized molecular dynamics at constant pressure [10]. Negative heat capacity in nuclear multifragmentation has also been observed in a canonical model [11]. In a microcanonical framework, Chomaz *et al.* [6] and D'Agostino *et al.* [12] obtained negative specific heat from fluctuation analysis, which has been widely claimed as indicating a first-order phase transition in nuclei. Exploiting the standard Clausius-Clapeyron equation for an evaporating liquid drop, Moretto *et al.* [13] find evidence of negative specific heat at constant pressure only when the binding energy per nucleon of the drop increases with mass number. In the nuclear context, from the binding energy curve, the mass number A of the drop is then less than $\sim$60. This maximum can, however, be controlled by inhibiting the Coulomb contribution, confining the evaporated nucleus in a box [14]. The analyses in Refs. [13,14] and the conclusions thereof have been achieved at the cost of some simplifying assumptions; namely, the system has been assumed to have only one component, the vapor phase is assumed to consist of monomers, and the transition is taken implicitly to be first order. For a one-component finite system, it is straightforward to find that the Clausius-Clapeyron equation may be written as

$$\frac{dP}{dT}(v_g - v_l) = (s_g - s_l) + \frac{dA_l}{dT}\left(\frac{\partial \mu_l}{\partial A_l} + \frac{\partial \mu_g}{\partial A_g}\right), \qquad (1)$$

where v, s, A, and μ refer to the specific volume, specific entropy, mass, and chemical potential for the liquid (l) and gas (g) phases, respectively, with $A_l + A_g = A_0$, the number of particles in the system. The last term is nonzero owing to the presence of the surface and is proportional to $A_l^{-1/3}$ (assuming the surface energy of the gas is negligible); it has been neglected in the analyses of [13,14]. In addition, for a simplistic analysis, the temperature of the system is taken to be much smaller compared to the binding energy per particle; this may not be typically the case here.

Mean-field models have often been employed to explore liquid-gas phase transition in infinite and finite nuclear systems. In this model, the phase transition is found to be continuous, both for asymmetric nuclear matter [15,16] and also for finite nuclei [17,18]. Though approximate, the model serves the purpose of giving an orientation for understanding some important features of the liquid-gas phase transition. It may therefore be worthwhile to undertake a full numerical calculation to explore whether the anomalous features in the caloric curve or in the specific heat persist, relaxing the constraints imposed in Refs. [13,14]. We make such an attempt in this paper. Moreover, the vapor phase may not consist of only monomers, but may contain various clusters along with

the nucleons; the influence of clusters on the caloric curve has also been explored.

II. THE MODEL

The model employed in the present calculation is in the framework of mean-field theory. The excited nucleus is viewed as a charged liquid drop composed of N_0 neutrons and Z_0 protons with mass number $A_0 = N_0 + Z_0$. In its journey from the liquid to the gas phase, the depleted nucleus is taken to be in complete thermodynamic equilibrium with its own emanated vapor so that the total number of neutrons and protons are conserved. To keep the description on a simpler pedestal, we first consider nucleonic vapor only. Besides nucleons, the vapor may contain clusters that would alter the equilibrium conditions, which will be reflected on the caloric curve and the resulting heat capacity. In this section we present some details of the methodology followed under these two conditions.

A. Nucleonic vapor

The framework for studying the liquid-gas phase transition for a heated nuclear liquid drop in equilibrium with the nucleonic vapor has been described in some detail in Ref. [17]. For simplicity, the mutual Coulomb interaction between liquid and gas was ignored there; in the present calculations this is taken into account. For the sake of completeness, we present here the relevant features of the model. The phase coexistence is governed by the Gibb's conditions:

$$\begin{aligned} P_l &= P_g, \\ \mu_n^l &= \mu_n^g, \\ \mu_p^l &= \mu_p^g, \end{aligned} \tag{2}$$

that is, the pressure and the chemical potentials of neutrons and protons are the same in both the liquid (l) and the gas (g) phase. This model has some resemblance to the one used by Lee and Mekjian [18], who studied the phase surface associated with a liquid-gas phase transition by incorporating the role of Coulomb and surface effects. However, they considered a fixed spherical volume at a chosen pressure and mapped the liquid-gas coexistence region by varying the density and proton concentration. Their results therefore do not pertain to a particular finite nuclear system and may not correctly describe the subtle nuances of a phase transition in a given finite system in a mean-field theory.

The total free energy of the nuclear system (in a single phase) at temperature T is taken as

$$F = A_0 f_{\rm nm}(\rho, X_0, T) + F_c + F_{\rm surf}, \tag{3}$$

where $f_{\rm nm}(\rho, X_0, T)$ is the free energy per particle of infinite nuclear matter at the same density ρ and neutron-proton asymmetry $X_0[= (N_0 - Z_0)/A_0]$ of the total system, F_c is the Coulomb free energy, and $F_{\rm surf}$ is the temperature- and asymmetry-dependent surface free energy. The free energy of infinite nuclear matter is evaluated with the SkM* interaction in the finite-temperature Thomas-Fermi framework. The detailed expressions for the free energies are given in the appendix.

In the liquid-gas coexistence region, the free energy $F_{\rm co}$ is

$$F_{\rm co} = F^l + F^g + F_c, \tag{4}$$

where F^l and F^g are the respective free energies of the liquid and the gas phase in the absence of the Coulomb interaction and F_c here represents the total Coulomb free energy of the system in the mixed phase. The free energy F^l is

$$F^l = A_l f_{\rm nm}(\rho^l, X^l, T) + F^l_{\rm surf}, \tag{5}$$

with A_l, ρ^l, and X^l as the nucleon number, density, and neutron-proton asymmetry in the liquid phase, respectively. The expression for F^g has the same form as given in Eq. (5) but here the surface free energy is neglected because of the very low density of the gas.

Because of its thermal motion, the liquid drop may be located anywhere within the spherical freeze-out volume. The Coulomb free energy F_c then depends on the distance d of the center of the liquid drop from the center of the freeze-out volume; this dependence is, however, very weak, as will be discussed in Sec. II B. The Coulomb free energy of the liquid part is taken to be that of a uniformly charged sphere of radius $R_l = r_l A_l^{1/3}$; the radius parameter r_l is related to the liquid density ρ^l as $r_l = 1/(\frac{4}{3}\pi\rho^l)^{1/3}$. The gas is taken to be uniformly distributed in the whole spherical freeze-out volume excluding the volume occupied by the liquid drop. The total Coulomb free energy is then given by

$$\begin{aligned} F_c = \frac{3}{5}e^2 &\left[\frac{Z_l^2}{R_l} + \frac{Z_g^2}{R}\left(\frac{V_l + V_g}{V_g}\right)^2 - \frac{Z_g^2}{R_l}\left(\frac{V_l}{V_g}\right)^2\right] \\ &+ \frac{3}{2}\frac{Z_g e}{R^3 - R_l^3}\left(Z_l e - Z_g e\frac{V_l}{V_g}\right)\left(R^2 - R_l^2 - \frac{1}{3}d^2\right), \end{aligned} \tag{6}$$

with Z_l, Z_g as the proton numbers and V_l, V_g as the volumes in the liquid and gas phase, respectively. The radius R of the freeze-out volume V_f $(= V_l + V_g)$ can be obtained from the densities and particle numbers in the two phases as obtained from the thermodynamic equilibrium conditions and conservation of neutron and proton numbers and is given by

$$\frac{4}{3}\pi R^3 = \frac{A_l}{\rho^l} + \frac{A_g}{\rho^g}. \tag{7}$$

It may be pointed out that Eq. (6) with $d = 0$ reduces to the same as that used in Ref. [19] for the two-step uniform density profile.

The surface free energy of the liquid part is taken as

$$F^l_{\rm surf} = \sigma(X^l, T) A_l^{2/3}, \tag{8}$$

where the temperature- and asymmetry-dependent surface energy coefficient $\sigma(X, T)$ is

$$\sigma(X, T) = [\sigma(0, 0) - a_s X^2]\left(1 + \frac{3}{2}\frac{T}{T_c}\right)\left(1 - \frac{T}{T_c}\right)^{3/2}, \tag{9}$$

which is obtained by considering semi-infinite nuclear matter in equilibrium with the nucleonic vapor at the relevant temperature and asymmetry [20]. The values of the surface energy coefficient of semi-infinite symmetric nuclear matter in its ground state, $\sigma(0, 0)$, the surface asymmetry coefficient a_s,

and the critical temperature T_c for the SkM* interaction are taken to be 17.51, 38.6, and 14.61 MeV, respectively [21]. In our model, at a given temperature or pressure, the number conservation and the thermodynamic equilibrium constraints provide a natural confining volume for the vapor phase in the coexistence region.

The unknown quantities for a given liquid-drop size A_l are the number of nucleons in the gas, A_g, the neutron-proton asymmetries X^l and X^g for the liquid and gas phases, and their respective densities ρ^l and ρ^g. The quantities A_g and X^g are determined from conservation of baryon number and of total isospin, respectively. The three remaining unknown quantities are determined by using the conditions given by Eq. (2) and employing the Newton-Raphson method. With the knowledge of these quantities the free energy and hence all the relevant observables can be evaluated.

B. Clusterized vapor

For a given A_l and with the guess values for X^l, ρ^l, and ρ^g [to be refined through iteration to satisfy Eq. (2)], the volume of the gas, V_g, and the number of neutrons and protons in that gas are known. With the knowledge of the freeze-out volume V_g and the neutron and proton number, the statistical multifragmentation model can be employed to find the multiplicities of the various fragments created out of the vapor phase at the chosen temperature. We take recourse to the grand-canonical model; in this model, the multiplicity n_i for the ith species of the generated fragments is given by

$$n_i = V_g \frac{mA_i}{2\pi\hbar^2\beta}\phi_i(\beta)\exp\left[-\beta\left(V_c^i - B_i - \mu_n N_i - \mu_p Z_i\right)\right], \tag{10}$$

where β is the inverse of temperature T; m is the nucleon mass; A_i, N_i, and Z_i are the mass, neutron, and charge numbers of the fragmenting species i; the B_i's are the binding energies of the generated species; and μ's are the nucleonic chemical potentials. The internal partition function $\phi_i(\beta)$ for species i with $A_i > 4$ is taken as

$$\phi_i(\beta) = \int_{\varepsilon_1^i}^{\varepsilon_2^i} d\varepsilon^* \rho_i(\varepsilon^*) e^{-\beta\varepsilon^*}. \tag{11}$$

Here ε_1^i is the lowest excited state and ε_2^i is the lowest particle-decay threshold of the ith species. In our calculations, these energy limits are taken to be the same for all the species with $\varepsilon_1 = 2$ MeV and $\varepsilon_2 = 8$ MeV. For the density of states, $\rho_i(\varepsilon^*)$, the Bethe level density expression,

$$\rho_i(\varepsilon^*) = \frac{6^{1/4}}{12}\frac{g_0}{(g_0\varepsilon^*)^{5/4}}\exp\left(2\sqrt{\frac{A_i\varepsilon^*}{10}}\right), \tag{12}$$

is used with $g_0 = 3A_i/4\pi^2$. For $A_i \leqslant 4$, $\phi_i(\beta)$ is taken to be unity. The single-particle Coulomb potential V_c^i is evaluated in the complementary fragment approximation [22,23] with the appropriate liquid and vapor charge distributions. The chemical potentials so generated may not be the same as those of the liquid phase. The chemical and mechanical equilibrium between the liquid and the clusterized vapor phase are obtained through an iterative procedure (Newton-Raphson method) by varying X^l, ρ^l, and ρ^g.

For simplicity the nuclear interaction among the fragments are neglected. This is insignificant owing to the large freeze-out volume. The pressure of the vapor phase is taken to be that of a perfect gas corrected for the Coulomb interaction given by

$$P_g = MT/V_g + \Delta P_g, \tag{13}$$

where M is the total fragment multiplicity in the gas phase and ΔP_g is the correction to the perfect gas pressure because of the Coulomb interaction. It is given by

$$\Delta P_g = -\frac{\partial V_c}{\partial V_g}, \tag{14}$$

where V_c is the Coulomb interaction energy of the system excluding the Coulomb self-energies of the clusters in the vapor phase; these self-energies are included in the B_i's. For the evaluation of the mutual interaction part (between liquid and vapor) in V_c, the charge distribution in the vapor phase is taken to be uniformly distributed in the volume V_g. This corresponds to an ensemble-averaged value if the clusters are randomly distributed within V_g in an event. The treatment of the liquid phase is the same as that described in Sec. II A.

The excitation energy of the system is evaluated from the energy balance condition

$$-B + E^* = \frac{3}{2}MT - \sum n_i B_i + \sum n_i \langle E_i^* \rangle + E_l + V_c. \tag{15}$$

Here B is the ground-state binding energy of the system, $\langle E_i^* \rangle$ is the average excitation energy of the ith species, and E_l is the energy of the liquid drop (excluding the Coulomb energy). The free energy of the vapor phase is the sum of the free energies of the fragments generated in this phase, including the contribution from their thermal motion. The detailed expressions are given in Ref. [1]. The expression corresponding to Eq. (15) for the case of monomeric vapor is obtained by dropping the second and third terms on the right-hand side and replacing M by A_g, the number of nucleons in the vapor. The energy of the excited liquid drop, E_l, is the sum of the contributions from the volume, Coulomb, and surface terms. The expression for the volume term is given in the appendix. The Coulomb energy is the same as the Coulomb free energy as it has no explicit temperature dependence. The surface energy $E_{\rm surf}^l$ is given by

$$E_{\rm surf}^l = F_{\rm surf}^l - T\left(\frac{\partial F_{\rm surf}^l}{\partial T}\right)_V. \tag{16}$$

III. RESULTS AND DISCUSSION

To explore the characteristics of phase transition in finite nuclei, we have chosen three representative systems, namely, ^{40}Ca, ^{150}Re, and ^{150}Nd. The symmetric systems ^{40}Ca and ^{150}Re are chosen to study the mass dependence, whereas the isobaric pairs ^{150}Re and ^{150}Nd offer the means to study the effects of asymmetry on the properties of the phase transition. To discern the effect of the long-range Coulomb interaction, calculations are also done both with and without this interaction.

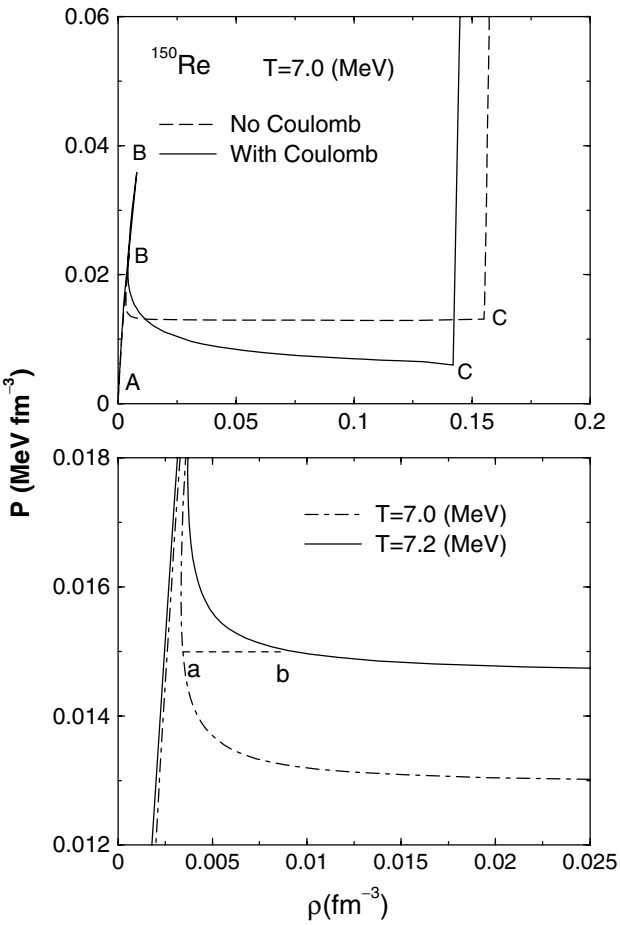

FIG. 1. The isotherms for the system ^{150}Re at $T = 7.0$ MeV with and without the Coulomb interaction (top panel) and at $T = 7.0$ and 7.2 MeV with Coulomb off in a narrow density interval (bottom panel). For the horizontal line *a*–*b*, see text.

The distance d of the center of the liquid drop from that of the freeze-out volume may vary from 0 to some maximum value $d_{\max}$. The latter corresponds to the surface of the drop touching the boundary of the freeze-out volume. The reduction in F_c as d is increased from 0 to $d_{\max}$ is very small; it is only a few percent, typically less than 4% of F_c. The results calculated with these two extreme values of d are practically indistinguishable, so we report calculations taking $d = 0$.

In this section we present the results of our calculations, first for the nucleonic vapor and then for the clusterized vapor.

A. Nucleonic vapor

In Fig. 1 (top panel), the isotherm for the symmetric nucleus ^{150}Re at $T = 7$ MeV is displayed. The full line refers to the results with the Coulomb interaction included, the dashed line corresponds to those without the Coulomb term. The lines (full or dashed) are obtained by exploiting the thermodynamic equilibrium conditions with the constraints of baryon number and isospin conservation and thus correspond to the fully physical region. The high-density side where the pressure rises very sharply with density (beyond point C) is the fully liquid phase. The wing from B to A and to further lower densities corresponds to the fully gas phase. The region from B to C is the region of liquid-gas phase coexistence. Symmetric nuclear matter behaves like a one-component system; the phase transition there occurs at a constant pressure. Without the Coulomb interaction even a symmetric finite nucleus (like ^{150}Re) does not behave like a one-component system because of the presence of the surface; the pressure changes, though weakly, along the phase transition. At constant pressure the transition then occurs over a finite temperature interval and the transition is thus *continuous*. With the introduction of the Coulomb interaction this effect is more pronounced. The isotherms obtained here display a Van der Waals type of loop; this kind of behavior has been observed earlier in an exact calculation for finite systems by Katsura [24] and Hill [25]. As mentioned in Refs. [24,25], the loop results from the interfacial (surface) effects between the two phases. The isotherms for the same system (^{150}Re) with the Coulomb interaction switched off are displayed in the lower panel of the figure in a narrower (P, ρ) interval at two nearby temperatures. One finds that for this system the pressure decreases with increasing density in the coexistence region. At constant pressure this may lead to a negative heat capacity c_p. At a fixed pressure, say, $P \sim 0.015$ MeV fm^{-3}, as the temperature of the system is increased from 7 to 7.2 MeV, the density changes from that at point *a* to a higher density at point *b*, leading to a negative isobaric volume expansion coefficient $\alpha = \frac{1}{V}(\partial V/\partial T)_P$. Since $c_p = c_v + \alpha V T (\partial P/\partial T)_V$ and $(\partial P/\partial T)_V$ is positive as seen in the figure, $c_p < c_v$ and under suitable conditions (as met in our calculations), it can be negative.

The isotherms for the asymmetric system ^{150}Nd at $T = 7$ MeV with and without the inclusion of the Coulomb interaction are shown in Fig. 2. Unlike the symmetric system ^{150}Re, here with the increase in density, the pressure initially decreases and then increases in the coexistence region. It appears that this difference in the behavior of the isotherms is a reflection of the asymmetry effect. To confirm this, we have done calculations for two isotopes of Ca, ^{40}Ca and ^{50}Ca, at $T = 7$ MeV with the Coulomb interaction. The asymmetry effect is apparent, as is displayed in Fig. 3. For clarity, the looping near the onset of the vapor phase is shown magnified in the inset in Fig. 2. As the temperature is increased, the phase coexistence region shrinks and points B and C set closer and at a certain temperature (the critical temperature T_c) they merge. The magnitudes of the critical parameters, namely, the temperature, pressure, and density, for the system ^{150}Nd are 13.1, 0.174, and 0.050 (all in MeV-fm units), respectively.

The variation of the liquid proton fraction Y^l $(= Z_l/A_l)$ at constant pressure is shown as a function of the mass number A_l of the depleting drop in the coexistence phase in the upper two panels of Fig. 4 for the systems ^{150}Re and ^{150}Nd. The calculations are representative and are done with the Coulomb interaction on at a constant pressure $P = 0.0014$ MeV fm^{-3}. In all the panels in this figure, the dashed lines refer to results with the monomeric vapor phase and the full lines correspond to those with the clusterized vapor phase. The variation of Y^l with A_l in the two systems differs somewhat. The nucleus ^{150}Re being highly proton-rich initially sheds off more protons to sustain chemical equilibrium with reduction in Y^l whereas

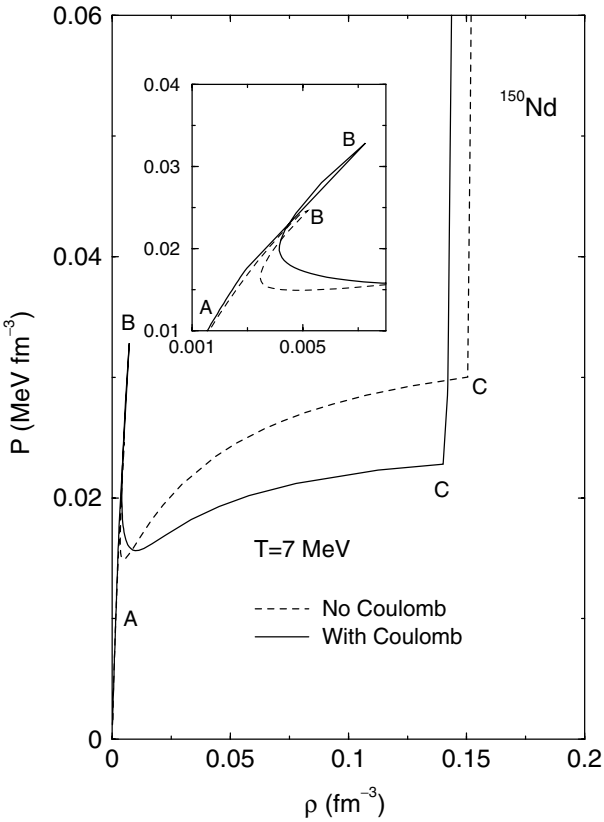

FIG. 2. The isotherms for the system ^{150}Nd with and without the Coulomb interaction. The inset magnifies the loop in a narrow density region.

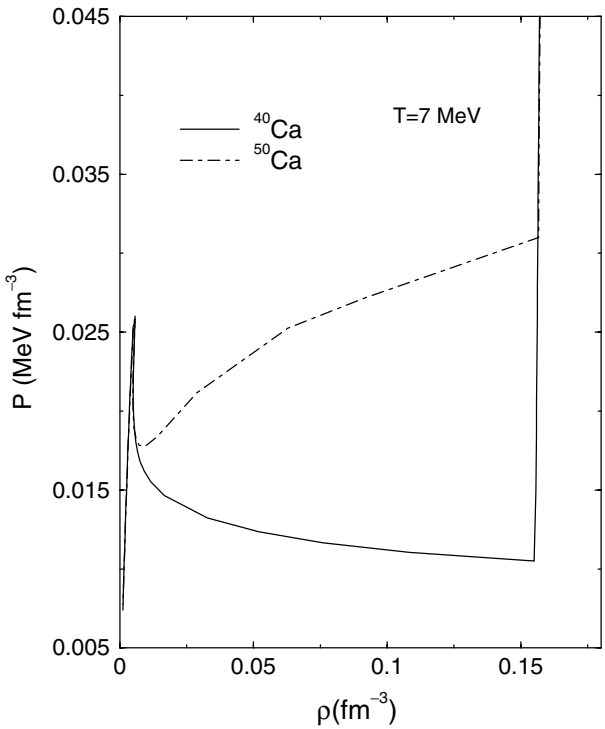

FIG. 3. The isotherms for the nuclei ^{40}Ca and ^{50}Ca at $T = 7$ MeV with the Coulomb interaction.

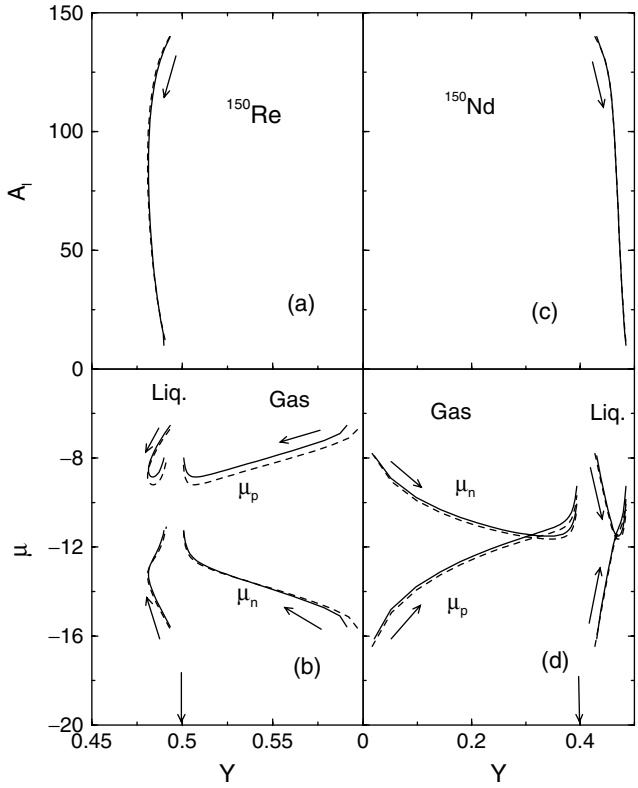

FIG. 4. The proton fraction Y^l of the liquid drop as a function of its depleting mass number A_l (upper panels). The neutron and proton chemical potentials in the liquid and gas phase as a function of the proton fraction in the respective phases (lower panels). The liquid and gas phase results are well separated and are marked in the figure. The vertical arrows on the abscissa show the proton fraction of the total system. The results correspond to constant pressure $P =$ 0.0014 MeV fm^{-3}.

for the more neutron-rich nucleus ^{150}Nd, the proton fraction in the liquid drop increases monotonically with its reduction in size. These results are seen to be insensitive to the particular choice of the vapor phase.

To maintain chemical equilibrium in the two phases, the neutron and proton chemical potentials along the coexistence line behave in a relatively complex fashion; they are displayed in the bottom panels of Fig. 4 as a function of the proton fraction in the respective phases. The vertical arrows on the abscissa mark the proton fraction of the total system. The direction of the arrow along a curve signifies depletion of the liquid phase, that is, the direction of increasing excitation energy. The thick lines represent the results for protons and the thin lines are those for the neutrons. The results for the liquid and gas phases are well demarcated and are labeled in the figure. The proton fractions in the two phases are quite different, indicating isospin distillation [26] in the coexistence phase. This is more prominent in the asymmetric system (^{150}Nd). In contrast to the neutron-rich gas phase for the asymmetric system, the symmetric nucleus ^{150}Re has a proton-rich gas phase. The results again are seen to be almost independent of the choice of the constituents of the vapor phase we have taken.

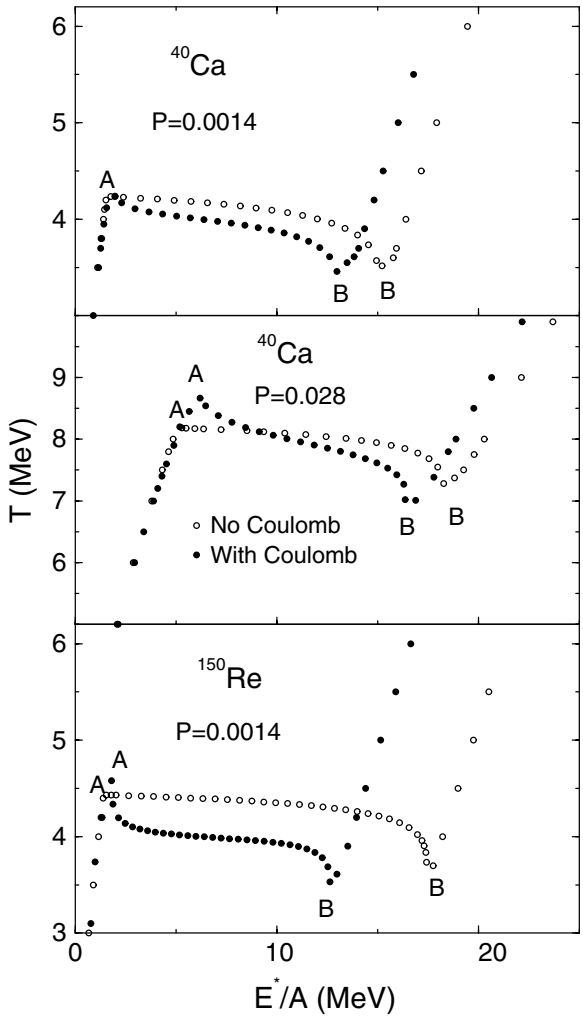

FIG. 5. The caloric curve for the system ^{40}Ca at $P = 0.0014$ MeV fm^{-3} with (filled circles) and without (open circles) the Coulomb interaction (top panel). The middle panel displays the same at $P = 0.028$ MeV fm^{-3}. The bottom panel is the same as in the top panel, but for the system ^{150}Re.

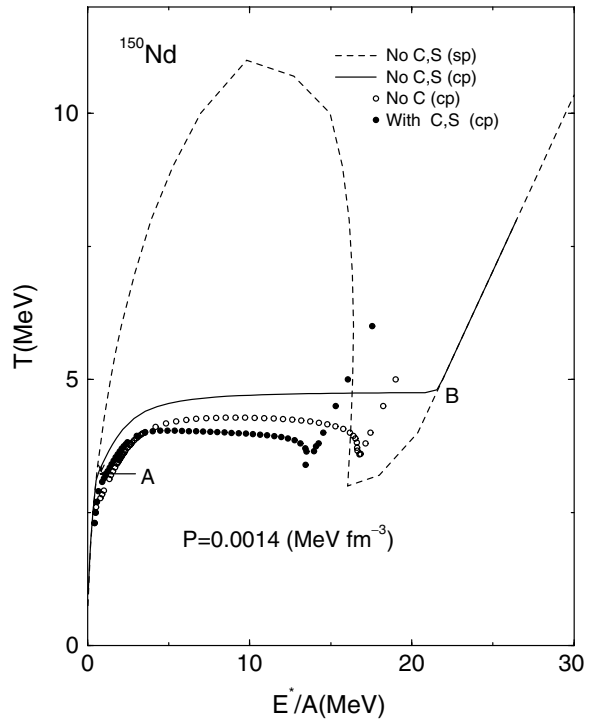

FIG. 6. The caloric curves for the system ^{150}Nd at $P = 0.0014$ MeV fm^{-3}. The dashed line is obtained after switching off the Coulomb (C) and the surface (S) effects in the single phase (sp), the full line refers to that with the coexistence phase (cp), the open circles correspond to the one after switching on the surface effect, and the filled circles refer to caloric curve with both Coulomb and surface on.

The calculated caloric curves at constant pressure for the symmetric systems ^{40}Ca and ^{150}Re are displayed in Fig. 5 with the Coulomb interaction switched on and off. The upper panel corresponds to a pressure $P = 0.0014$ MeV fm^{-3} and the middle panel is for a pressure 20 times higher ($P = 0.028$ MeV fm^{-3}) for the lighter system ^{40}Ca. The caloric curves show some anomalous features. At excitation energies lower than the one marked by point A, the system is in the fully liquid phase; here the rise in excitation with temperature is like that of a Fermi gas. The region A to B corresponds to the liquid-vapor coexistence. As the system moves from A to B, the nucleus increasingly gets depleted in size with emanation of vapor; beyond B, it is in the fully vaporized state. The caloric curves for the heavier system ^{150}Re with the Coulomb interaction switched on and off are shown in the bottom panel at a pressure $P = 0.0014$ MeV fm^{-3}. The characteristics of these caloric curves are very similar to those for the lighter system ^{40}Ca. For both the lighter and the heavier symmetric nuclei we consider, it is seen that the temperature decreases with the excitation energy over the whole coexistence phase; this would lead to negative heat capacity. It is further noted that the negative slope of the caloric curve is amplified with the inclusion of the Coulomb interaction.

Figure 6 displays the caloric curves for the asymmetric system ^{150}Nd at $P = 0.0014$ MeV fm^{-3} with and without the inclusion of the Coulomb interaction. The presence of a Van der Waals type of loop in the isotherms for finite systems for fully physical results obtained with consideration of complete thermodynamic equilibrium between the liquid and the gas phase has been mentioned before. The presence of this loop is expected to produce a negative sloping caloric curve. To elaborate this further, calculations have been performed by switching off both the Coulomb (C) and the surface (S) effects. This actually corresponds to the case of infinite asymmetric nuclear matter. The dashed line represents the results of considering a single phase (sp) over the whole excitation energy domain considered. Here the temperature passes through a maximum and a minimum very similar to the variation of pressure with density at constant temperature, the slope of the caloric curve being negative in between the maximum and the minimum. For an infinite system the loop in the isotherm is absent with appropriate consideration of the liquid-vapor coexistence phase (cp) and the negative slope in the caloric curve is then expected to be absent here. This is

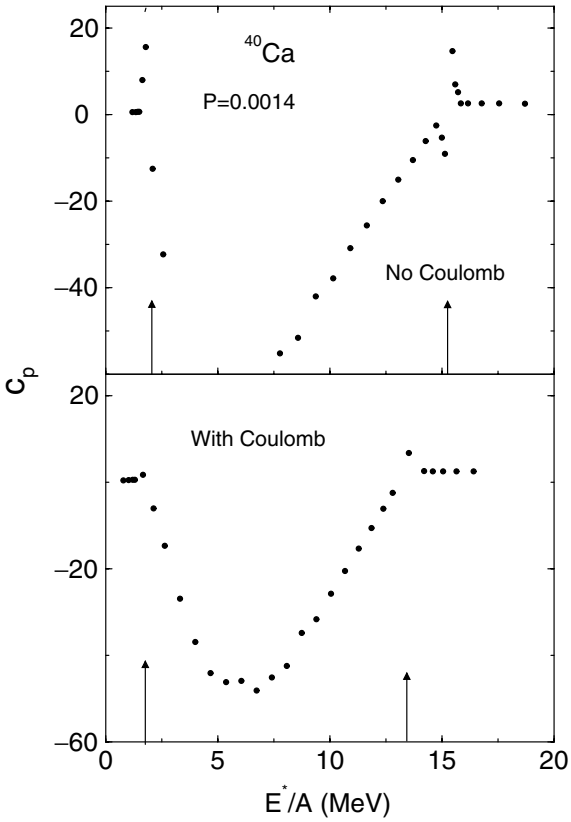

FIG. 7. Heat capacity at constant pressure for the system ^{40}Ca with (bottom panel) and without (top panel) the Coulomb interaction. The arrows indicate the points of discontinuity.

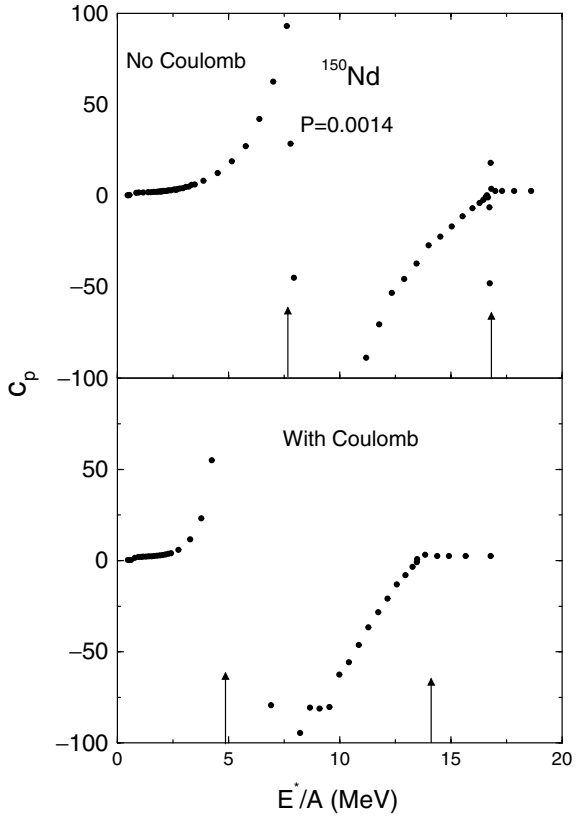

FIG. 8. Same as Fig. 7 for the system ^{150}Nd.

really the case, as can be seen from the caloric curve shown by the full line where the excitation energy domain between points A and B refer to the liquid-vapor coexistence region. The caloric curves with successive inclusion of the surface and the Coulomb effect are shown by the open circles and the filled circles, respectively. The characteristic features of these caloric curves are grossly the same as those of the symmetric systems ^{40}Ca and ^{150}Re discussed before. However, one distinct difference is noticeable. Unlike the symmetric systems ^{40}Ca or ^{150}Re, where, whether with Coulomb on or off, the negative heat capacity extends over the whole coexistence phase, for the asymmetric system ^{150}Nd, this occurs for $A_l < 30$ with Coulomb off and at $A_l \sim 100$ with Coulumb on.

The caloric curve results presented here show that both the Coulomb interaction and asymmetry play important roles in determining its detailed characteristics. The asymmetry tends to produce a caloric curve with a positive slope. This is evident from the observation that, for an asymmetric system like ^{150}Nd, the negative slope occurs only after some nucleons (predominantly neutrons) are evaporated and the residual nucleus is closer to a symmetric one, whereas for a symmetric system like ^{40}Ca or ^{150}Re, the slope is negative throughout the coexistence phase. The Coulomb interaction, in contrast, tends to enhance the negative slope, as is clear from the results presented in Figs.5 and 6. The asymmetry of the evaporated gas is enhanced with the asymmetry of the nucleus whereas it is reduced by the Coulomb interaction. The delicate dependence of the temperature and excitation energy on the asymmetry in the two phases to maintain phase coexistence seems to be responsible for the features of the caloric curve as seen here.

The specific heat at constant pressure $c_p[= \frac{1}{A}\frac{d}{dT}(E + PV)_P]$ for the systems ^{40}Ca and ^{150}Nd at $P = 0.0014$ MeV fm^{-3} are displayed in Figs. 7 and 8 as a function of excitation energy per particle. The upper panels correspond to results with Coulomb off; the lower panels show the same with Coulomb on. There are two discontinuities in the specific heat, one at lower excitation and the other at higher excitation (marked by arrows), and the specific heat is negative within this range. These discontinuities refer to the change in the sign of the slopes of the caloric curves. The discontinuity at the higher excitation always occurs at the point of complete vaporization of the system; the one at the lower excitation depends on the system (symmetric or asymmetric) and on the choice of the interaction (Coulomb on or off). Negative specific heat occurs in a small temperature interval, typically ∼1.0 to 1.5 MeV for the cases we have considered.

Analysis of fluctuations of kinetic energy of the fragments [12] and the direct measurement of the caloric curve as well as the analyses of a number of other observables by the TAMU group [27] indicate that the heat capacity is negative only in a small excitation energy domain, around 3–7 MeV/nucleon in Ref. [12] and around 5–6 MeV/nucleon in Ref. [27]. Our calculated results contradict this finding as the calculated specific heat at constant pressure remains negative up to excitation energy as high as 14 MeV/nucleon. This may

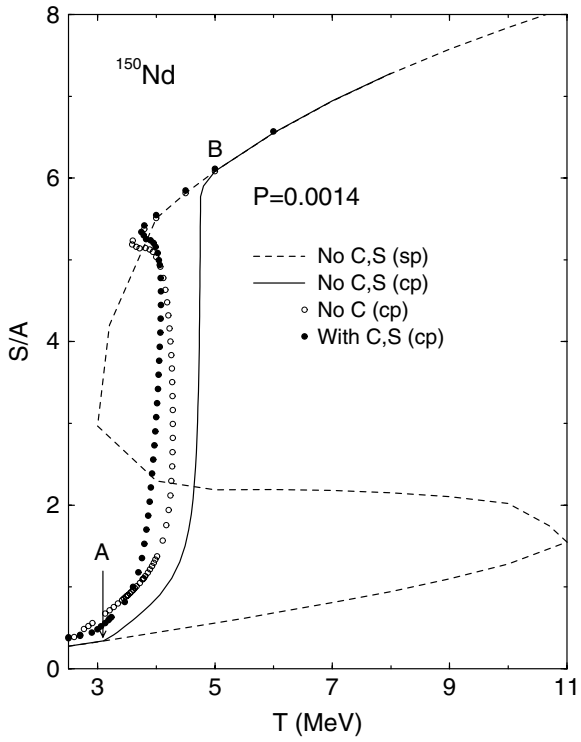

FIG. 9. Entropy per particle, S/A, as a function of temperature for the system ^{150}Nd at $P = 0.0014$ MeV fm^{-3}. The notation is the same as in Fig. 6.

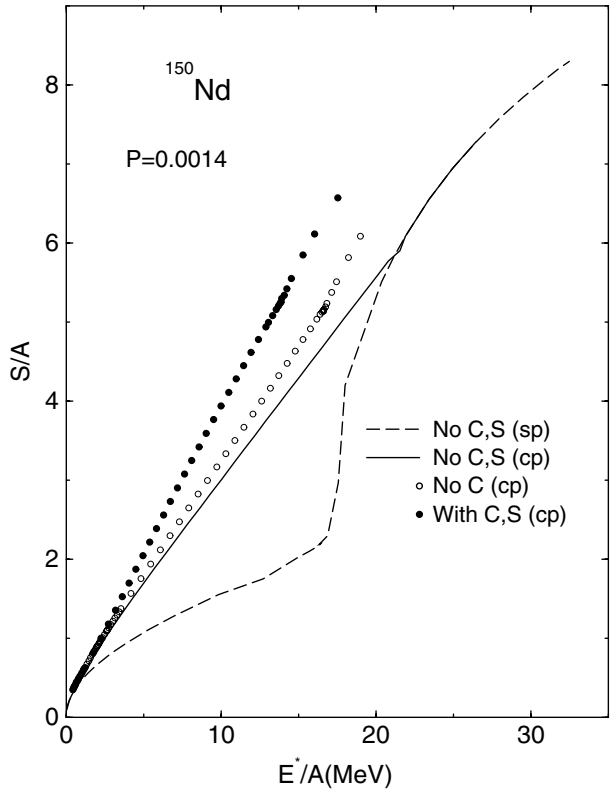

FIG. 10. Entropy per particle as a function of excitation energy per particle, E^*/A, for the same case as in Fig. 9. The notation is the same as in Fig. 6.

be traced back partly to the inadequacy of the mean-field model we adopt that masks the fluctuations. Furthermore, in our model the vapor phase consists of monomers only. In reality nucleons are emitted along with various fragments. This would modify the equilibrium conditions such as pressure, chemical potentials, and temperature for a given excitation energy of the fragmenting system and in turn the caloric curve and the associated heat capacity would be affected. This aspect is dealt with in Sec. III B. The actual conditions prevailing in a fragmentation scenario may be neither isobaric nor isochoric. This may also modify the behavior of the specific heat appreciably, leaving some room for uncertainties in the comparison of the existing theoretical results with the experimental findings.

In Fig. 9, the calculated entropy per particle, S/A, at constant pressure $P = 0.0014$ MeV fm^{-3} is shown as a function of temperature for the system ^{150}Nd. The notation used is the same as in Fig. 6. The results for the single-phase calculation (dashed line) for infinite asymmetric matter having neutron-proton asymmetry the same as that of ^{150}Nd have some anomalous behavior. Over a wide range of temperature it is seen that the entropy increases with a decrease of temperature. This unphysical character vanishes with the appropriate inclusion of the liquid-vapor coexistence phase, as shown by the full line, the region A to B being the region of coexistence for the two phases. With the inclusion of the surface and/or the Coulomb effect, the entropy-temperature curve for ^{150}Nd displays a negative slope even with the inclusion of the coexistence phase, as shown by the open circles and the filled circles. The change in entropy does not show any discontinuity with temperature though there are marked changes in slope; the phase transition is then continuous. The temperature window for the persistence of the negative slope of the entropy curve is the same as that seen in the caloric curve. The dependence of entropy on the excitation energy at constant pressure is shown in Fig. 10 for the different cases studied, as mentioned in the context of Fig. 9. It is seen that for all the cases entropy increases monotonically with excitation energy, as expected.

It may also be worth mentioning that liquid-gas coexistence may occur with a bubble configuration in which the gas is enclosed in a shell of liquid. In nuclear matter, the minimum size for a possible bubble to occur is similar to the size of a heavy nucleus [28]. For finite systems, our calculation shows that the drop configuration is favored over the bubble. The free energy for the bubble configuration is found to be much higher compared to that of the corresponding drop configuration with the same A_l. This is due to the large surface free energy in the bubble configuration with two liquid surfaces having large radii.

B. Clusterized vapor

For the clusterized vapor, the results for the caloric curve are displayed for the symmetric system ^{150}Re (top panel) and that for the asymmetric system ^{150}Nd (bottom panel) at $P = 0.0014$ MeV fm^{-3} in Fig. 11. To discern the effect of clusters,

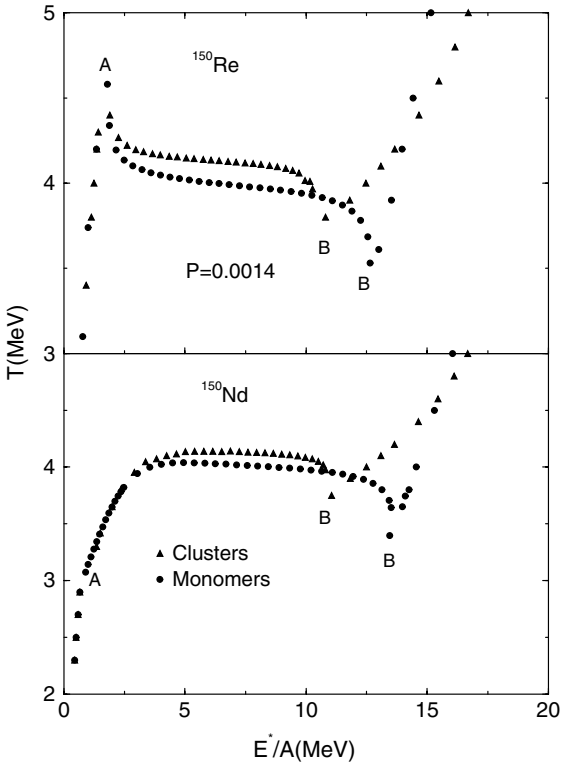

FIG. 11. Caloric curve with monomers (filled circles) and clusters (filled triangles) in the vapor phase for the systems ^{150}Re (top panel) and ^{150}Nd (bottom panel).

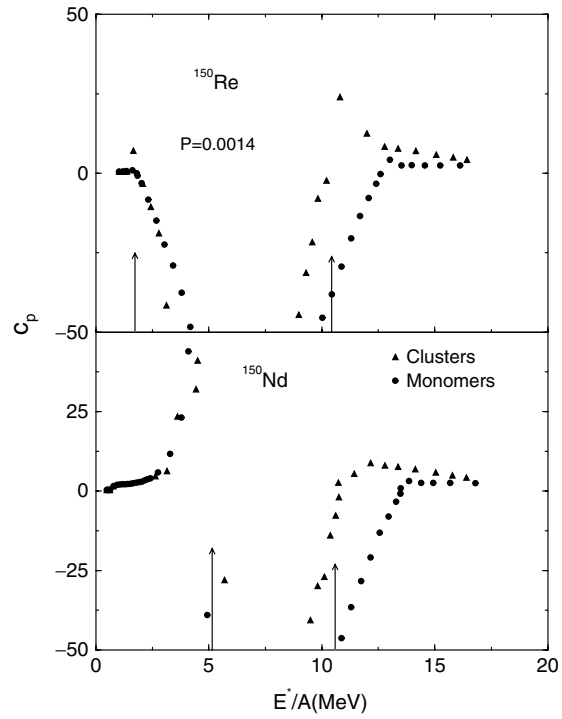

FIG. 12. Heat capacity at constant pressure for the system ^{150}Re (top panel) and ^{150}Nd (bottom panel). The arrows indicate the points of discontinuity.

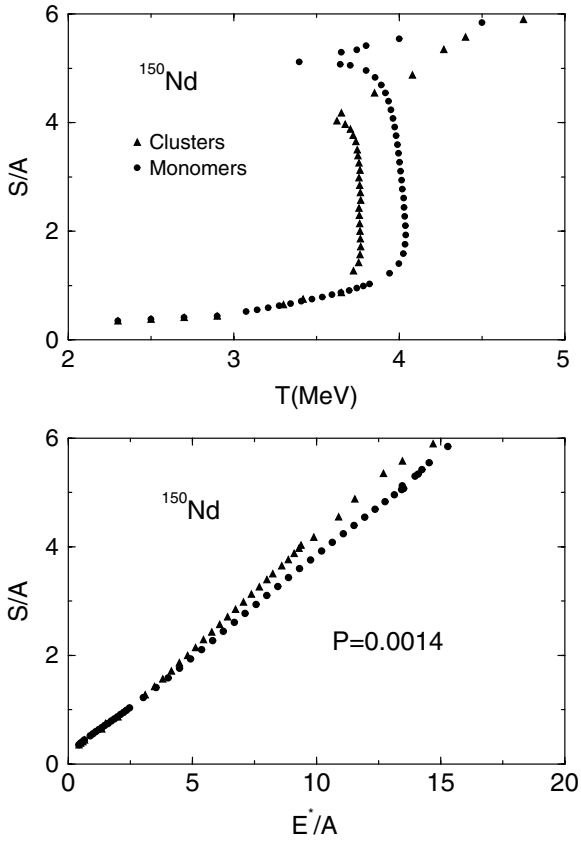

FIG. 13. Entropy as a function of temperature (top panel) and excitation energy (bottom panel) for the system ^{150}Nd at $P = 0.0014$ MeV fm^{-3}.

the caloric curves for nucleonic vapor are also presented (filled circles) along with those for the clusterized vapor (filled triangles). As in Fig. 5, the region A to B corresponds to the liquid-vapor coexistence region. The chemical potential profiles with proton fraction in the coexistence phase do not differ much for the two choices of the vapor phase, as is seen in Fig. 4. The basic features of the caloric curve are also not altered with the inclusion of clusters. Thus all the remarks for the caloric curve made previously are also valid here. One important difference, however, lies in the occurrence of complete vaporization of the system at a relatively lower excitation energy with consideration of clusters. This is self-evident because the clusters are bound systems. With increasing excitation energy, clusters dissolve into nucleons and the caloric curves tend to merge.

In Fig. 12 the heat capacities at constant pressure (c_p) are displayed corresponding to the caloric curves shown in Fig. 11. The arrows indicate the positions of excitation energies corresponding to the change in sign of c_p and between the arrows it is negative. The upper bound of the excitation energy for c_p being negative is reduced significantly (from ∼14 to 10 MeV) with the inclusion of clusters for reasons already stated in connection with the caloric curve. However, this reduction is not sufficient to match the experimental findings.

The entropy for ^{150}Nd as a function of temperature is shown in the top panel of Fig. 13. As in the case of monomeric vapor,

the back bending (i.e., increase of entropy with reduction in temperature) persists in a narrow temperature interval even after inclusion of fragments. The bottom panel shows the entropy as a function of excitation energy for the same system. With clusterized vapor, the entropy is a little larger compared to monomeric vapor, showing that the clusterized configuration is more favorable.

IV. CONCLUDING REMARKS

Within a mean-field framework, we have studied the liquid-gas phase transition in finite nuclei with exact conservation of baryon number and isospin. As in asymmetric nuclear matter, since at constant pressure the transition occurs over a finite temperature domain and because the entropy shows no discontinuity with temperature, we conclude that, in the model studied, the said transition in finite nuclei is continuous. However, unlike bulk systems, a Van der Waals type loop in the isotherm is observed in the coexistence region because of finite size effects. This loop, arising from the thermodynamic equilibrium conditions, results in negative specific heat at constant pressure in a small temperature domain. Moretto *et al.* [14] find negative specific heat only for nuclei with $A \leqslant 60$; we find distinct evidence of negative specific heat for considerably heavier systems. In Ref. [14], the size of the system refers to the residual evaporated drop; this may be identified with the depleted drop of size A_l in our calculations rather than the total mass A_0 of the nucleus. Aside from this fact, the main reason for this discrepancy lies in the exact computation of the equilibrium configurations in the liquid and gas phase in our calculations. The presence of back bending in the caloric curve or a negative heat capacity in microcanonical or canonical formulations has been taken as tacit evidence that the liquid-vapor phase transition in finite nuclei is first order. In fact, there is evidence of a first-order phase transition in two-component systems [29] in multifragmentation calculations based on the statistical model. In the mean-field model, however, the fluctuations implied in the fragmentation calculations are absent, the phase transition is seen to be continuous, and a negative specific heat for finite nuclei is not incompatible with it. The qualitative features of the results remain the same if, instead of pure nucleonic vapor, vapor with clusters is considered. The important change with inclusion of cluster is the significant reduction in the maximum excitation energy (from around 14 to 10 MeV/nucleon) up to which the heat capacity is negative. This maximum excitation is still higher compared to the experimental finding ($\sim$7 MeV/nucleon); aside from the inadequacy of the mean-field model, a possible reason for this difference may be the nonisobaric and/or nonisochoric conditions under which fragmentation occurs.

ACKNOWLEDGMENTS

J. N. D. gratefully acknowledges the kind hospitality at the Cyclotron Institute at Texas A&M University where the work was partially done. J. N. D. and S. K. S. acknowledge the Department of Science & Technology and the Council of Scientific and Industrial Research of the Government of India, respectively, for financial support. This work was supported in part by the U.S. National Science Foundation under Grant No. PHY-0355200, by the U.S. Department of Energy under Grant No. DE-FG03- 93ER40773, and by the Robert A. Welch Foundation.

APPENDIX: EVALUATION OF FREE ENERGY

The different components occurring in the total free energy F in the single phase given in Eq. 3 are the volume, Coulomb, and surface terms. The explicit expressions for them are as follows.

(i) **Volume term:** The free energy per particle of infinite asymmetric nuclear matter, $f_{\rm nm}(\rho, X_0, T)$, is

$$f_{\rm nm} = e_{\rm nm} - T s_{\rm nm}, \tag{A1}$$

where $e_{\rm nm}$ and $s_{\rm nm}$ are the energy and entropy, respectively, per particle. The energy $e_{\rm nm}$ is given by

$$e_{\rm nm} = \varepsilon_{\rm nm}/\rho, \tag{A2}$$

where the energy density is

$$\varepsilon_{\rm nm} = \sum_{q=n,p} \frac{\hbar^2}{2m_q}\tau_q + \varepsilon_i, \tag{A3}$$

where m_q is the nucleon mass and n or p stand for neutron or proton. Here ε_i is the interaction energy density. The terms under the summation represent the kinetic energy density expressed as

$$\tau_q = \frac{2m_q}{\hbar^2} A_{T,q} T J_{3/2}(\eta_q). \tag{A4}$$

The fugacity η_q is related to the nucleon density as

$$\rho_q = A_{T,q} J_{1/2}(\eta_q), \tag{A5}$$

with

$$A_{T,q} = \frac{1}{2\pi^2}\left(\frac{2m_q T}{\hbar^2}\right)^{3/2}, \tag{A6}$$

and J's are the Fermi integrals given by

$$J_k(\eta) = \int_0^\infty \frac{x^k}{1+e^{(x-\eta)}} dx. \tag{A7}$$

For the SkM* interaction, the interaction energy density for nuclear matter is [30]

$$\begin{aligned}\varepsilon_i = {} & \tfrac{1}{2}t_0\left[\left(1+\tfrac{1}{2}x_0\right)\rho^2 - \left(x_0+\tfrac{1}{2}\right)\left(\rho_n^2+\rho_p^2\right)\right] \\ & + \tfrac{1}{12}t_3\rho^\alpha\left[\rho^2 - \tfrac{1}{2}\left(\rho_n^2+\rho_p^2\right)\right] + \tfrac{1}{4}(t_1+t_2)\tau\rho \\ & + \tfrac{1}{8}(t_2-t_1)(\tau_n\rho_n + \tau_p\rho_p),\end{aligned} \tag{A8}$$

with $\tau = \tau_n + \tau_p$ and $\rho = \rho_n + \rho_p$. The values of the parameters in Eq. (A8) are given in Ref. [30]. The entropy per nucleon is

$$s_{\rm nm} = \frac{1}{\rho}\sum_q \left[\frac{5}{3}A_{T,q}J_{3/2}(\eta_q) - \eta_q\rho_q\right]. \tag{A9}$$

(ii) **Coulomb term:** The Coulomb free energy is taken to be that of a uniformly charged sphere,

$$F_c = \tfrac{3}{5} Z_0^2 e^2 / R, \tag{A10}$$

where $Z_0 e$ is the total charge of the system with radius R.

(iii) **Surface term:** The surface free energy $F_{\rm surf}$ is given by

$$F_{\rm surf} = \sigma(X_0, T) A_0^{2/3}, \tag{A11}$$

where the expression for the surface energy coefficient $\sigma(X, T)$ is given by Eq. (9).

For the vapor phase, the expressions for volume and Coulomb energy have the same form; the surface free energy is taken to be zero because of its very low density.

[1] J. P. Bondorf, R. Donangelo, I. N. Mishustin, and H. Schulz, Nucl. Phys. **A444**, 460 (1985).
[2] J. P. Bondorf, A. S. Botvina, A. S. Iljinov, I. N. Mishustin, and K. Sneppen, Phys. Rep. **257**, 130 (1995).
[3] D. H. E. Gross, Rep. Prog. Phys. **53**, 605 (1990).
[4] X. Campi, J. Phys. A **19**, L917 (1986).
[5] S. Dasgupta, A. Z. Mekjian, and M. B. Tsang, Adv. Nucl. Phys. **26**, 91 (2001), and references therein.
[6] P. Chomaz, V. Duflot, and F. Gulminelli, Phys. Rev. Lett. **85**, 3587 (2000).
[7] J. N. De, S. DasGupta, S. Shlomo, and S. K. Samaddar, Phys. Rev. C **55**, R1641 (1997).
[8] J. Pochodzalla *et al*., Phys. Rev. Lett. **75**, 1040 (1995).
[9] J. B. Elliot *et al*., Phys. Lett. **B418**, 34 (1998).
[10] T. Furuta and A. Ono, Prog. Theor. Phys. Suppl. **156**, 147 (2004).
[11] C. B. Das, S. DasGupta, and A. Z. Mekjian, Phys. Rev. C **68**, 014607 (2003).
[12] M. D'Agostino *et al*., Phys. Lett. **B473**, 219 (2000).
[13] L. G. Moretto, J. B. Elliott, L. Phair, and G. J. Wozniak, Phys. Rev. C **66**, 041601(R) (2002).
[14] L. G. Moretto, J. B. Elliott, and L. Phair, Phys. Rev. C **68**, 061602(R) (2003).
[15] M. Barranco and J. R. Buchler, Phys. Rev. C **22**, 1729 (1980).
[16] H. Müller and B. D. Serot, Phys. Rev. C **52**, 2072 (1995).
[17] T. Sil, S. K. Samaddar, J. N. De, and S. Shlomo, Phys. Rev. C **69**, 014602 (2004).
[18] S. J. Lee and A. Z. Mekjian, Phys. Rev. C **63**, 044605 (2001).
[19] P. Pawlowski, Phys. Rev. C **65**, 044615 (2002).
[20] D. G. Ravenhall, C. J. Pethik, and J. M. Lattimer, Nucl. Phys. **A407**, 571 (1983).
[21] K. Kolehmainen, M. Prakash, J. M. Lattimer, and J. Treiner, Nucl. Phys. **A439**, 535 (1985).
[22] D. H. E. Gross, L. Satpathy, M. T. Chung, and M. Satpathy, Z. Phys. A **309**, 41 (1982).
[23] L. Satpathy, M. Mishra, A. Das, and M. Satpathy, Phys. Lett. **B237**, 181 (1990).
[24] S. Katsura, J. Chem. Phys. **22**, 1277 (1954).
[25] T. L. Hill, J. Chem. Phys. **23**, 812 (1955).
[26] H. S. Xu *et al*., Phys. Rev. Lett. **85**, 716 (2000).
[27] Y. G. Ma *et al*., Phys. Rev. C **69**, 031604(R) (2004).
[28] S. Shlomo and V. M. Kolomietz, Rep. Prog. Phys. **68**, 1 (2005).
[29] C. B. Das, S. DasGupta, W. G. Lynch, A. Z. Mekjian, and M. B. Tsang, Phys. Rep. **406**, 1 (2005).
[30] M. Brack, C. Guet, and H. B. Hakansson, Phys. Rep. **123**, 275 (1985).